Acta Geodyn. Geomater., Vol. 22, No. 2 (218), 277–290, 2025
DOI: 10.13168/AGG.2025.0019
journal homepage: https://www.irsm.cas.cz/acta

ORIGINAL PAPER

SPATIOTEMPORAL SEA LEVEL CHANGE AROUND JAPAN SEA FROM SATELLITE ALTIMETRY AND IN SITU OBSERVATION WITH EOF ANALYSIS FROM 1993 TO 2020

Haodong LIU [1] * and Yilin CHEN [2]

[1] *School of Civil and Surveying & Mapping Engineering, Jiangxi University of Science and Technology, Ganzhou 341000, China.*
[2] *School of foreign languages, Jiangxi University of Science and Technology, Ganzhou 341000, China.*

**Corresponding author's e-mail:* dong_h_l@163.com

ARTICLE INFO

Article history:
Received 26 February 2025
Accepted 13 June 2025
Available online 30 June 2025

Keywords:
Sea level change
Satellite altimetry
Tide gauges
GNSS
Empirical orthogonal function analysis

ABSTRACT

We investigate the spatiotemporal characteristics of sea level change (SLC) in Japan's territories by analyzing tide gauge (TG) records and satellite altimetry (SA) data from 1993 to 2020. The analysis reveals that the relative sea level change (RSLC) rate in Japan is 2.20 ± 0.62 mm/a, while satellite altimetry (SA) data calculate an absolute sea level change rate (ASLC) of 3.13 ± 1.66 mm/a. Additionally, some TG stations show significant sea level subsidence rates, primarily attributed to vertical land movement (VLM), particularly the land uplift effect in localized regions, leading to negative RSLC. After correcting for VLM, the recalculated SLC rate is 3.77 ±.26 mm/a, which is consistent with the value of 3.4 mm/a reported by the Japan Meteorological Agency. Through Empirical Orthogonal Function (EOF) analysis, the primary spatial patterns of change in both SA and TG data exhibit a high degree of consistency, with the first mode contributing 80.24 % and 82.95 % of the variance, respectively. The first mode of EOF for the coastal sea level represents a simultaneous (SLC) along the whole Japanese coast and the second mode is closely related to the Kuroshio Large Meander (LM). Further, extract the dominant components of sea level variation, and denoising was performed on the TG data. Compared to the Raw data, the denoised data showed a root mean square (RMS) error reduction of 6.98 mm on average, with uncertainty decreasing by 0.25 mm/a. These results provide important insights for more accurate SLC trend estimation.

1. INTRODUCTION

During the satellite altimetry era (since 1993), independent estimate indicates global mean sea level (GMSL) rise of 3.2 ± 0.3 mm/a over 1993–2021 (Dangendorf et al., 2024; He et al., 2024; Wang et al., 2025), 3.3 ± 0.4 mm/a over 1993–2023 (Hamlington et al., 2024). According to the sixth assessment report of the Intergovernmental Panel on Climate, GMSL increased by 0.15–0.25 m over the period 1901 to 2018 at an average rate of 1.3–2.2 mm/a, and the rate in the GMSL rise has accelerated since the 1960s to 3.2–4.2 mm/a for the period 2006 to 2018 (IPCC 2021). The main factors contributing to the GMSL rise are ocean thermal expansion and inflow of water mass due to land ice melt and changes in land water storage (Clark et al., 2015; Palmer et al., 2020). However, the sea level rise is neither temporally nor spatially uniform because, in addition to the above factors, regional sea level is influenced by other factors such as changes in ocean circulation and atmospheric forcing (Qiu et al., 2015; Carson et al., 2017; Woodworth et al., 2019; Hamlington et al., 2020; Han et al., 2025).

Japan is located on the western rim of the Pacific Ocean, and the mechanisms behind sea level change (SLC) in this region are complex. Given the unique seafloor topography along Japan's coastline and its heightened sensitivity to rising sea levels, it is particularly important to continuously monitor changes in sea level and their associated spatial and temporal characteristics. SLC has long been recorded by tide gauge (TG) stations. A TG station is a land-attached device that integrates a set of monitoring sensors to observe and record the relative water-land movement. Specifically, it continuously measures the height of sea level relative to a vertical datum (Thompson et al., 2016; Kleinherenbrink et al., 2018; Adebisi et al., 2021), referred to as relative sea level change (RSLC). In coastal areas, RSLC collectively combines the effects of vertical land motion (VLM) and absolute sea level change (ASLC). VLM reflects elevation changes of land surface in the form of either subsidence or uplift (Wöppelmann and Marcos, 2016; Zhu et al., 2023; Zhu et al., 2024). VLM is a major issue in Japan and is now monitored in real time (Geospatial Information Authority of Japan, 2018a). They also provide "long-term" information on crustal movement, meaning up to 10 years. Different from RSLC, ASLC is not influenced by the local VLM and refers to the height variations of the ocean surface. Furthermore, Numerous studies (Senjyu et al., 1999; Sasaki et al., 2013; Uchida and Imawaki, 2008; Usui et al., 2017; Zhang and Church, 2012; Sasaki et al., 2017; Wu et al., 2022; Sakamoto et al., 2005; Ito et al.,

Cite this article as: Liu H, Chen Y: Spatiotemporal sea level change around Japan Sea from satellite altimetry and in situ observation with EOF analysis from 1993 to 2020. Acta Geodyn. Geomater., 22, No. 2 (218), 277–290, 2025. DOI: 10.13168/AGG.2025.0019

2004; Bessières et al., 2013; Boretti, 2024) have investigated interannual and decadal sea level variations associated with the Japanese coastline. In particular, the works of Sasaki et al. (2014), Yasuda and Sakurai (2006), and Nakano et al. (2023) have provided valuable insights into these changes, contributing significantly to the understanding of regional sea level dynamics over different time scales. The analysis of multi-decadal or century-long TG records presents numerous challenges in accurately estimating SLC and its associated uncertainty (Chepurin et al., 2014). A meticulous approach is essential, requiring careful modeling of diverse processes (e.g., seasonal variations) and considering the temporally correlated noises intrinsic to these measurements. These noises can impact the analysis of various time series, including geodetic time series (Burgette et al., 2013; He et al., 2017; He et al., 2022a; Montillet and Bos, 2019), particularly affecting observations recorded by TG. However, in order to accurately estimate the SLC, previous studies have primarily focused on denoising time series data, often treating the data without considering the underlying oceanic signal mechanism.

This study employs the Empirical Orthogonal Function (EOF) method to analyze oceanic data, providing a more comprehensive approach by capturing the spatial and temporal patterns inherent in the signal. This method is a mathematical dimensionality reduction technique that can reflect the main characteristics of SLCs on the spatial scale. As a common technique for data analysis, the EOF method can analyze and extract the change of long-term sea level variations, which is better for investigating the causes of SLCs. The advantage of this method is that a typical field is determined by the characteristics of time series of variables, instead of being determined artificially in advance, so it can better reflect the basic structure of the field (Wallace et al., 1972; Hannachi et al., 2004; Lian et al., 2012; Kim et al., 2015). It can decompose the irregularly distributed sites in a limited area, and the decomposed spatial structure has a clear physical significance. Compared with a fully data driven approach denoising method (e.g., Empirical Mode Decomposition (EMD), which adaptively decomposes the signal into multiple intrinsic mode functions (IMFs) without relying on prior physical models or mechanisms, but instead based on the local features of the data itself for decomposition and denoising) (Boudraa et al., 2004; Kabir and Shahnaz, 2012), the principal component (PC) decomposition can better extract the consistent changes of sea level in the study area. By conducting a comparative analysis of the meanings represented by each mode, this approach allows for a more accurate identification and removal of noise components from the TG data, followed by the estimation of the SLC. The method aims to mitigate the impact of noise on the estimation of SLC rates, thereby providing a more precise evaluation of SLC.

The remainder of the paper is organized as follows. Section 2 provides brief descriptions on the SA, TG data and GNSS observations used in this study. In Section 3 we use these approaches to estimate the SLC and VLM in Japan based on the analysis of SA, TG, GNSS and we conduct the EOF analysis of the Japanese coastal sea level by using both the SA and TG. Its mechanism is discussed in Section 3.3. Based on the analysis of physical mechanisms, the decomposed modes are used to denoise TG data and re-estimate RSLC, and compared with the EMD denoising results in Section 3.4. The findings from the present study are summarized in Conclusion.

2. DATA AND METHODS

2.1. TIDE GAUGE OBSERVATIONS

The TG data are provided by the Permanent Service for Mean Sea Level (PSMSL) (Holgate et al., 2013; https://psmsl.org), based on monthly average data in the RLR (Relative Long-term Records) format. The reference for this data is defined as approximately 7000 mm below the mean sea level to avoid negative RLR monthly values. We selected data from 22 TG stations located along the Japanese coastline. Figure 1 shows the spatial locations of these stations and such a selection is based on the following considerations. First, to obtain precise trends from continuous data, an observation period of 28 years (from 1993 to 2020) is used in this study. Second, TG stations exhibit a low missing data rate—approximately 1.45 % on average across the 22 sites used in our analysis. Third, most TG stations are co-located with GNSS reference stations within a 15 km radius (Bitharis et al., 2017). To analyze the spatiotemporal characteristics of the TG records, we applied EOF analysis, ensuring that the time series were continuous and consistent. For this purpose, we used monthly average sea level data from 1993 to 2020. After 1993, some TG station records were damaged, so we interpolated missing data. The RSL trend was first calculated using the TG data, and to explore the spatiotemporal characteristics of SLC, we performed data analysis on the detrended sea level records from the 22 TG stations. This approach allows for the investigation of both long-term and interannual sea level trends.

2.2. SEA SURFACE HEIGHT FROM SATELLITE ALTIMETRY

We used the daily products of GLOBAL_MULTIYEAR_PHY_001_030 (https://doi.org/10.48670/moi-00021) from the Copernicus Marine Environment Monitoring Service (CMEMS), covering the period from 1993 to 2020, which is defined on a standard regular grid at 1/12-degree resolution and covering approximately 8 km (He et al., 2022b; Huang et al., 2024). To investigate the SLC in SSH from SA, and to facilitate the exploitation of altimetry data at the coast, we used the concept of virtual altimetry stations developed and used by Cazenave et al. (2022) for the computation of

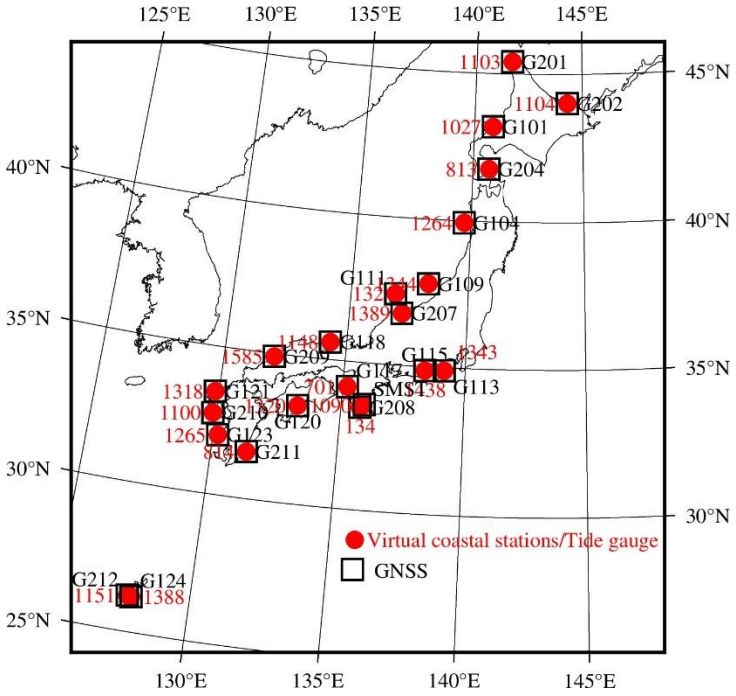

Fig. 1 Spatial distribution of the analyzed 22 stations along the coast of Japan.

sea level trends, a concept we implemented in our study. We determined the 22 virtual coastal stations around the coasts (also called virtual coastal stations with SA observations) based on the longitude and latitude of the TG from PSMSL, as illustrated in Figure 1.

2.3. GNSS DATA

The GNSS time series used in this study were acquired from Nevada Geodetic Laboratory (NGL, Blewitt et al., 2018; Hammond et al., 2021; http://geodesy.unr.edu). GNSS is a commonly used geodetic technique due to its high precision to monitor land motions (He et al, 2015; Ballu et al., 2019; Huang et al., 2025; Zhou et al., 2025). For comparison, we have analyzed the measurements from a total 22 of GNSS stations which are co-located at or close to a TG station along Japan (Fig. 1 and Table 1). There are two main issues involved in estimating VLM trends for TGs with GNSS time series. Firstly, many GNSS stations are not directly connected to TG stations. There is often a lack of regular leveling activities to monitor the relative VLM between the TG and GNSS stations. Therefore, to attenuate this effect, we use the GNSS stations neighboring the TG to estimate the VLM trend whose distances are shown in Table 1. Secondly, the VLM estimated from GNSS data should remain consistent throughout the entire period of the TG data. However, in practice, GNSS time series rarely satisfy this condition completely. We selected GNSS stations that are adjacent to the TG and have longer time series as correction data sources (see Table 1). When both conditions are met, the VLM detected by GNSS can be considered representative of the VLM at the TG reference point, assuming that the VLM is uniform across adjacent regions. This data can be used to correct the trends in RSLC (Bruni et al., 2022; Zhou et al., 2022).

2.4. EOF ANALYSIS

The EOFs, also known as a Principal Component Analysis (PCA), can be used to analyze the variance contribution of different components for extracting spatiotemporal features (Wallace et al., 1972; Halliwell et al., 1984; Hannachi, 2004; Wilks et al., 2011; He et al., 2015). The orthogonal basis is derived by computing the eigenvectors of a spatially weighted anomaly covariance matrix and the corresponding eigenvalues provide a measure of the percent variance explained by each pattern. Therefore, EOFs a space-time physical process can be represented mutually by orthogonal space patterns where the data variance is concentrated with the first pattern being responsible for the largest part of the variance, the second for the largest part of the remaining variance, and so on. We then write

$$X = (y_1, y_2 \cdots y_n) = \begin{bmatrix} y_{11} & \cdots & y_{1n} \\ y_{21} & \cdots & y_{2n} \\ \vdots & \ddots & \vdots \\ y_{m1} & \cdots & y_{mn} \end{bmatrix} \tag{1.1}$$

Where n is the number of TG stations, and m denotes the number of a time period. In addition, the covariance matrix B of time series is orthogonally decomposed as follows：

$$B = \frac{1}{m-1} X^T X \tag{1.2}$$

Table 1 Virtual coast station of satellite altimetry, tide gauge and co-located GNSS station used in this work.

Tide Gauge (1993~2020)	Lon	Lat	Data Gap (%)	Co-located GNSS	Data Span	Distance (km)	TG&GNSS Overlap (%)
132	136.90	37.41	3.87	G111	2003.42-2023.19	0.04	46.25
134	135.77	33.48	0.00	G208	2003.24-2023.19	0.02	48.73
701	135.19	34.14	0.00	G117	2003.44-2023.19	0.05	49.66
813	140.73	41.78	0.00	G204	2003.28-2023.19	0.05	51.40
814	131.41	31.58	0.00	G211	2003.40-2023.19	0.03	46.85
1027	140.86	43.21	0.00	G101	2003.42-2023.19	0.06	32.05
1090	135.90	33.56	0.00	SMST	2004.27-2022.97	4.39	40.58
1100	129.87	32.74	0.30	G210	2003.24-2022.62	0.02	49.64
1103	141.69	45.41	0.00	G201	2003.24-2023.19	0.03	51.08
1104	144.29	44.02	0.60	G202	2003.42-2023.19	0.05	51.39
1148	134.32	35.59	0.30	G118	2003.45-2023.19	0.04	48.76
1151	127.67	26.21	0.30	G212	2003.44-2023.19	0.04	49.28
1264	139.71	39.94	1.49	G104	2003.41-2023.19	0.22	51.50
1265	130.19	32.02	0.30	G123	2003.44-2023.19	0.07	32.63
1318	129.85	33.47	8.04	G121	2003.44-2023.19	0.03	38.32
1320	133.24	33.33	0.30	G120	2003.43-2023.19	0.07	50.22
1343	139.13	34.90	4.46	G113	2003.44-2023.19	0.06	32.74
1344	138.28	37.82	3.87	G109	2003.42-2023.19	0.03	52.86
1388	127.82	26.18	4.17	G124	2003.44-2023.19	0.09	50.91
1389	137.23	36.76	0.00	G207	2003.42-2023.19	0.04	50.05
1438	138.33	34.87	3.87	G115	2003.44-2023.19	0.05	52.18
1585	132.07	34.90	0.00	G209	2003.46-2023.19	0.04	46.44

$$B = EDE^{T} = \begin{bmatrix} \lambda_1 & \cdots & 0 \\ \vdots & \ddots & \vdots \\ 0 & \cdots & \lambda_n \end{bmatrix} \begin{bmatrix} e_1^T \\ e_2^T \\ \vdots \\ e_3^T \end{bmatrix} \quad (1.3)$$

where λ1 > λ2 > ⋯ > λn. The orthogonal decomposition of the space domain can be computed as the feature vector of $X^T X$, and the EOF value can then be obtained by normalizing the decomposition. In addition, the PC can be calculated in the time series according to the following expressions:

$$PC = XE \quad (1.4)$$

3. SEA LEVEL VARIABILITY ALONG THE JAPANESE COAST

3.1. SEA LEVEL CHANGE FROM SATELLITE ALTIMETRY

In order to estimate the sea level trends, we select the most appropriate noise model for each site based on the BIC-tp criterion (Bos et al., 2014; Peng et al., 2022). As indicated by the colored dots in Figure 2 and Table 2, the ASL along the coast of Japan generally shows an upward trend, although the rate of increase varies across different regions. Notably, the southeast coast experiences a higher rate of sea level rise compared with other regions. The ASLC along Japan's coastline ranges from 2.52 ± 0.45 mm/a to 4.61 ± 1.88 mm/a. Particularly, the 1090 TG located on the southeast coast of Japan records a significantly higher rate of sea level rise compared with other stations. The average ASLC rate across the 22 stations along Japan's coastline is 3.13 ± 1.66 mm/a, with the uncertainty range spanning from 0.40 to 3.32 mm/a, with a mean uncertainty of 1.66 mm/a as shown in Figure 3 and Table 2. The left panel of Figure 3 demonstrates a persistent increase in sea level along the Japanese coast, which is comparable to the GMSL trend of 3.3±0.40 mm/a form (https://sealevel.colorado.edu/index.php/data/2020rel1-0). Additionally, the sea level rise along the southeast coastal belt of Japan is greater than in other regions, which is consistent with previous studies suggesting that the Kuroshio Current is a contributing factor (Uchida et al., 2008; Sasaki et al., 2013; Sasaki et al., 2014). The schematic diagram from Sasaki et al. (2014, Fig. 11) illustrates the mechanism of sea level change (SLC) along the coast of Japan. The blue arrow indicates an incoming jet-trapped Rossby wave, while the gray arrow represents coastal waves generated in response to the incoming Rossby wave. The nature of the waves captured by the Kuroshio Current leads to significant SLC along the southeastern coast of Honshu. Moreover, as this region exhibits the highest population density in Japan, it remains particularly vulnerable to the impacts of sea-level rise.

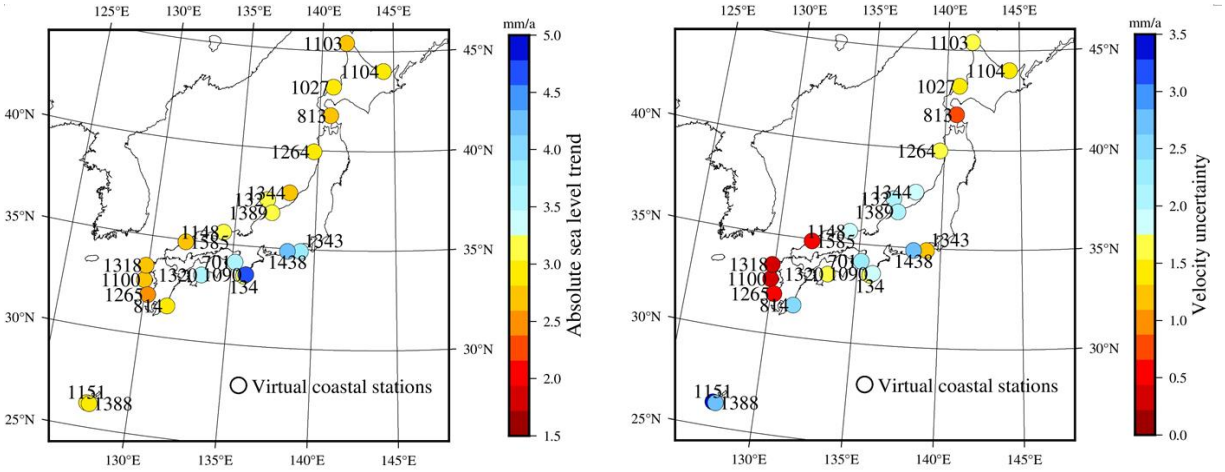

Fig. 2 Absolute sea level trend from satellite altimetry (left) and uncertainty (right) for the period 1993-2020.

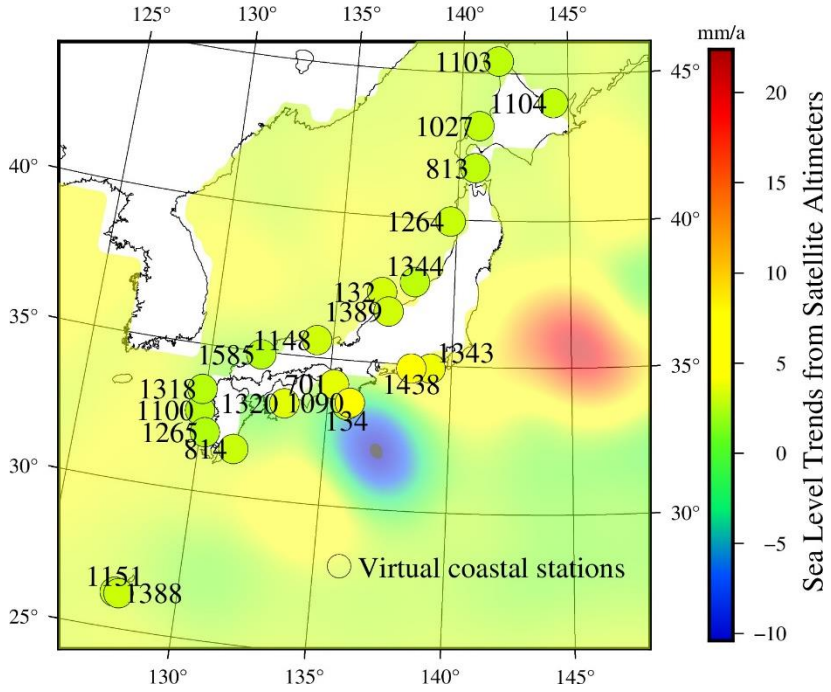

Fig. 3 Sea level trends from satellite altimeters (https://sealevel.colorado.edu/index.php/data/2020rel1-0) (color contours) and virtual station from this study (colored dots).

3.2. VLM IMPACT EVALUATION IN THE TIDE GAUGE OBSERVATION

This study utilizes monthly mean sea level data from 22 TG stations located in Japan's coastline, spanning the period from 1993 to 2020. The SLC for each station were calculated, revealing that the highest and lowest rates of change occur along the southeastern and northern coasts of Japan (Fig. 4), respectively. The uncertainty range for the rates varied from 0.34 to 1.68 mm/a, with an average value of 0.62 mm/a, as shown in Figure 4 (Bos et al., 2014; Huang et al., 2024). The range of RSLC along the Japanese coastline varied from -4.21 ± 0.56 mm/a to 7.37 ± 1.04 mm/a. The average RSL rise rate for the 22 stations along the coast of Japan was 2.20 ± 0.62 mm/a. It is important to note that, unlike SA measurements, the TG data includes information not only on SLC but also on VLM. Therefore, the SLC reflected by the TG data differ from the ASL measured by SA. To convert RSLC to ASLC, we applied a VLM correction to the RSL from the TG (Zhou et al., 2022; Bruni et al., 2023). The uncertainty is estimated as the square root of the quadratic sum of the respective uncertainties of the VLM and RSL trend, as both observations are independent (Pfeffer and Allemand, 2016). Specifically, VLM data from GNSS stations

Table 2 Sea level rise and vertical land motion at tide gauges (mm/a).

TG	TG	ASL SA	RSL TG	VLM	|VLM/SA|	Corr SA-TG	TG+GNSS	(TG+GNSS)-SA
WAJIMA	132	3.22±2.03	2.34±0.58	0.92±0.60	0.29	0.92	3.26±1.24	0.04
KUSHIMOTO	134	3.08±1.59	5.99±0.58	-3.11±0.75	1.01	0.79	2.88±1.28	-0.20
KAINAN	701	3.63±2.26	-0.44±0.64	4.83±0.11	1.33	0.79	4.39±1.06	0.76
HAKODATE I	813	2.78±0.87	-4.21±0.56	7.48±1.18	2.69	0.50	3.27±1.35	0.49
ABURATSU	814	2.99±2.61	3.44±0.47	-1.63±0.57	0.55	0.77	1.81±1.20	-1.18
OSHORO II	1027	2.82±1.44	0.58±0.34	3.18±1.07	1.13	0.75	3.76±1.27	0.94
URAGAMI	1090	4.61±1.88	7.37±1.04	-1.44±2.59	0.31	0.82	5.93±1.62	1.32
NAGASAKI	1100	2.63±0.41	4.18±0.62	-1.90±0.86	0.72	0.88	2.28±1.31	-0.35
WAKKANAI	1103	2.79±1.55	2.70±0.43	1.87±0.11	0.67	0.83	4.57±0.99	1.78
ABASHIRI	1104	2.84±1.47	0.69±0.50	4.35±0.49	1.53	0.72	5.04±1.19	2.20
TAJIRI	1148	3.11±1.91	5.34±0.51	-2.04±0.21	0.66	0.92	3.30±1.08	0.19
NAHA	1151	2.96±3.32	3.07±0.68	0.26±0.21	0.09	0.90	3.33±1.13	0.37
OGA	1264	2.98±1.66	-1.26±0.58	5.07±1.47	1.70	0.83	3.81±1.40	0.83
AKUNE	1265	2.52±0.45	3.16±0.45	0.15±2.04	0.06	0.86	3.31±1.45	0.79
KARIYA	1318	2.61±0.40	3.05±0.93	0.35±0.23	0.13	0.90	3.40±1.20	0.79
KURE I	1320	3.56±1.64	-0.91±0.69	5.62±0.57	1.58	0.77	4.71±1.26	1.15
ITO II	1343	3.86±1.27	-2.76±0.43	6.11±1.91	1.58	0.63	3.35±1.43	-0.51
OGI	1344	2.77±1.77	-1.84±0.59	6.50±1.52	2.35	0.76	4.66±1.41	1.89
OKINAWA	1388	3.03±2.73	3.06±0.69	0.60±0.19	0.20	0.88	3.66±1.13	0.63
TOYAMA	1389	3.13±2.08	3.70±0.37	0.98±0.56	0.31	0.93	4.68±1.16	1.55
YAIZU	1438	4.33±2.81	5.94±1.68	-1.77±0.54	0.41	0.88	4.17±1.43	-0.16
HAMADA II	1585	2.62±0.45	5.16±0.35	-1.89±0.20	0.72	0.90	3.27±1.02	0.65

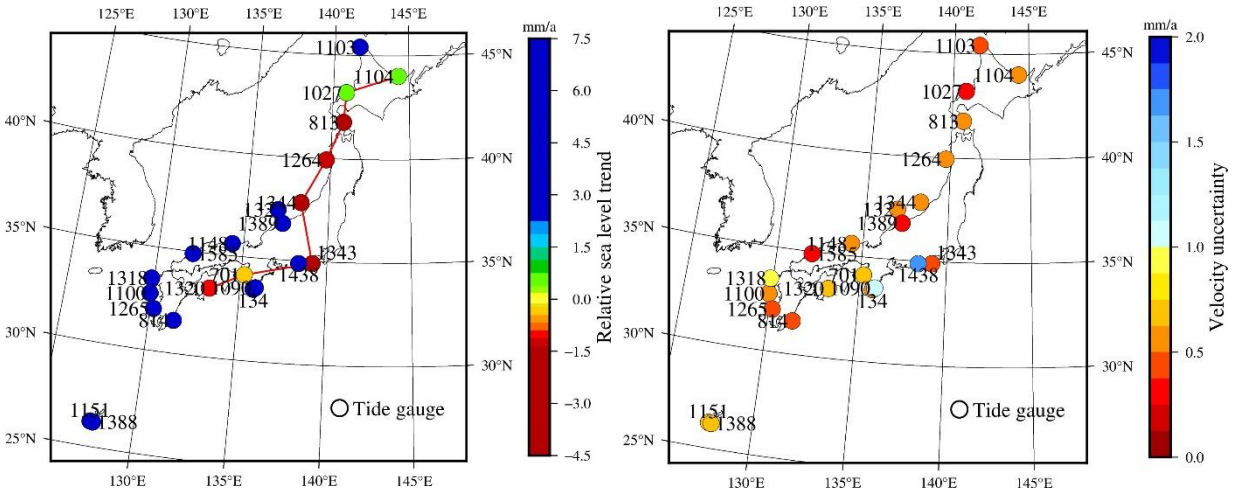

Fig. 4 Relative sea level trend from tide gauge data (left) and uncertainty (right) calculated for the period 1993-2020.

(provided by NGL) located near the TG stations were used to estimate the ASLC. GNSS stations with long-term records and located TG were selected as the data sources for the correction, as detailed in Table 1. Table 2 summarizes the VLM rate near the Japanese TG stations. The highest rates of VLM were recorded at the HAKODATE I station (7.48 ± 1.18 mm/a) and the OGI station (6.50 ± 1.52 mm/a), while both the KUSHIMOTO and TAJIRI stations experienced subsidence rates greater than 2 mm/a. These stations are often located in tectonically active regions, where sea-level records are significantly influenced by crustal deformation associated with the subduction of oceanic plates (Okuno et al., 2014). Table 2 also presents the ASLC rates derived from the analysis of TG and GNSS, and compares these with corresponding estimates from SA.

As illustrated in the figures, there are significant variations in the RSLC rates along the Japanese coastline. Eight stations (marked by the red lines in the left panel of Fig. 4) exhibit notably lower RSLC rates compared with the other stations, with six of these

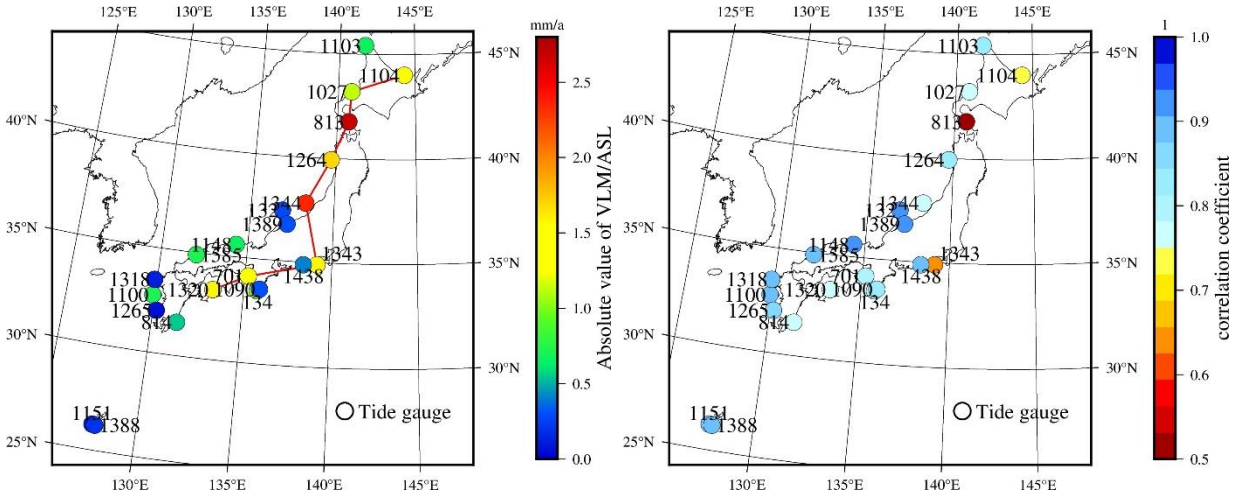

Fig. 5 Ratio of vertical land motion to absolute sea level velocity (left), and the correlation coefficient between monthly averaged satellite altimetry data (SSH) from 22 virtual stations (same latitude and longitude as the tide gauges) and the tide gauge recorded water level data (right).

Table 3 SA/TG variances, and accumulative total variances of different eigen structures.

PCs (100%)	TGEOF1	TGEOF2	SAEOF1	SAEOF2
Variances	82.95	5.16	80.24	6.43
Accumulative variances	82.95	88.11	80.24	86.67

stations showing negative values in RSLC. The change rates at these stations range from -4.21 ± 0.56 mm/a to 0.58 ± 0.34 mm/a. In order to investigate the cause of this phenomenon, we further analyzed the influence of VLM on these stations. The analysis revealed that these eight stations are strongly affected by VLM, with VLM intensities generally exceeding the ASL values by more than 1.1 times, as shown in the left panel of Figure 5 and Table 2. In ITO II station, the VLM values are even more than twice the magnitude of the ASL. The stronger VLM (uplift rates) has led to a reduction in the RSL change rates at these stations, with some even showing negative values. Additionally, the correlation coefficients between monthly mean SA and TG data, presented in the right panel of Figure 5 and Table 2, also support this finding. In regions with higher VLM, the correlation coefficients between the SA data and TG data are relatively lower. After applied VLM corrections to the RSL at these eight stations, the discrepancies with the ASLC derived from SA were reduced, further confirming the significant influence of VLM in these areas. Moreover, the corrected SLC rates for the TG stations were compared with the official data from the Japan Meteorological Agency (JMA). The corrected SLC rates ranged from 1.81 ± 1.20 mm/a to 5.93 ± 1.62 mm/a, with an average RSL rise rate of 3.77 ± 1.26 mm/a, which aligns with the JMA data with access of "https://www.data.jma.go.jp/kaiyou/english/sl_trend/sea_level_around_japan.html" (showing an average MSL rise rate of 3.4 mm/a for the period 2006–2018).

3.3. AN EOF ANALYSIS TO THE SEA LEVEL CHANGE

Based on the TG, SA data from 1993 to 2020, the variance explained by the first two PCs accounts for 88.81-86.67 % (see Table 3) of 22 eigenvectors. This can reflect the main changes in sea level trend at 22 TG stations in Japan. The spatial eigenvectors of 22 eigen structures and the corresponding time coefficients are show in Figures 6 and 7.

The first mode of the EOF of the interannual variation represents the simultaneous of sea levels along the Japanese coast. Figure 7b and Figueres 6a and 6c) show the time series of the PC and the horizontal pattern for the first EOF mode. The first mode explains more than 80 % of the sea level variability along the Japanese coast. The PC time series and the horizontal pattern of EOF1 for SA compares well with those for TG observation, indicating that SA captures the observed sea level variability well. The first EOF mode has the same sign at the all-TG stations (Figs. 6a and 6c), indicating that the first mode represents a simultaneous SLC along the whole Japanese coast. The amplitude of EOF1 is large along the south coast of Japan between the Boso Peninsula and Kyushu, and is relatively small along the Hokkaido coast. The correlation coefficient of the corresponding time coefficients is 0.89. The spatial eigenvectors of 22 eigen structures are shown in Figure 7a. The corresponding time coefficients are shown in Figure 7b. which indicates that the overall trend of the temporal and spatial variations is positive, with the south coast stations having the largest positive values. In terms of time coefficients, there is an obvious upward trend from 1993 to 2020 (Fig. 3).

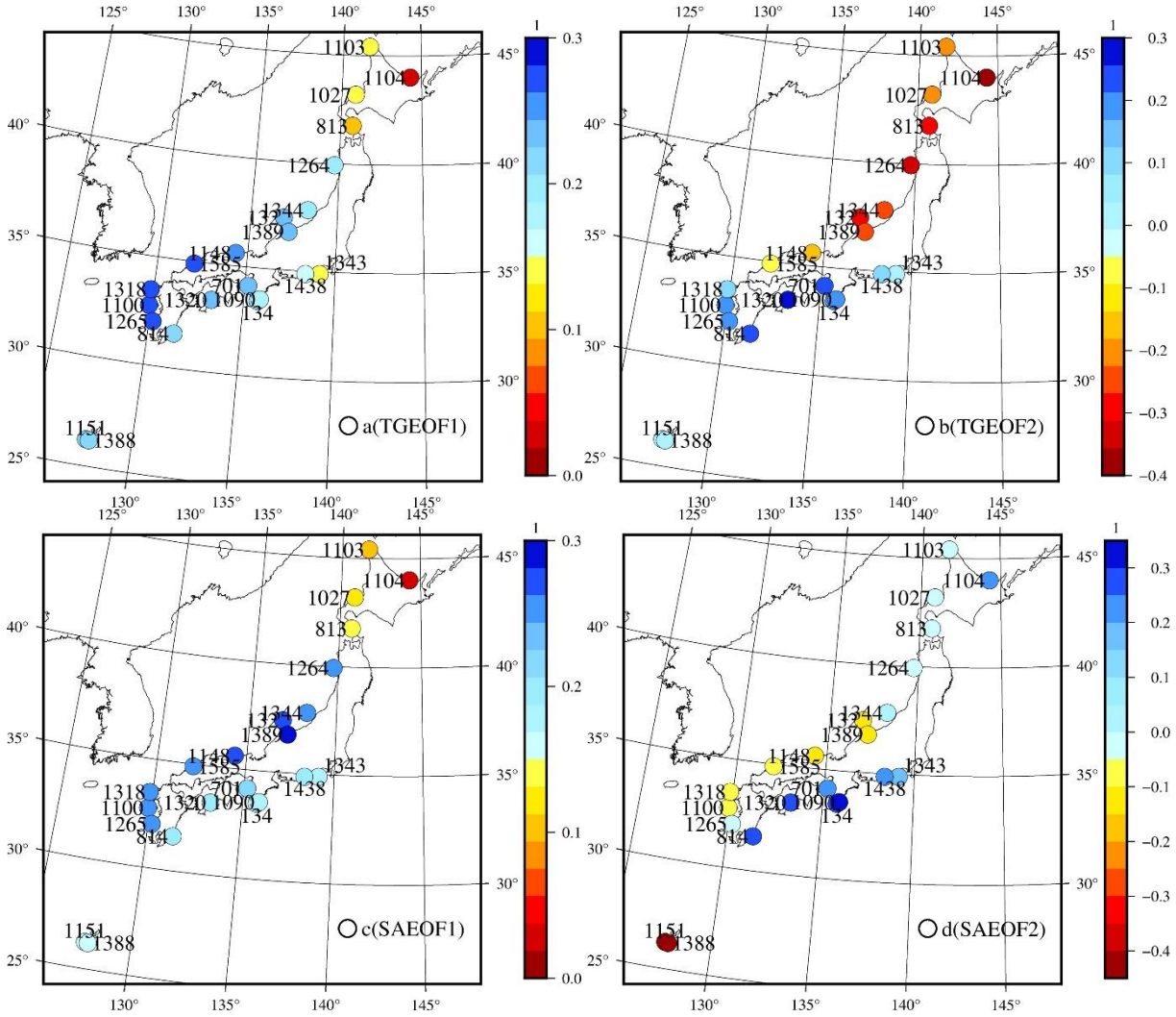

Fig. 6 Spatial distribution of eigenvectors of the first and second mode for the tide gauge (a, b) observation and satellite altimetry (c, d). Color indicates the amplitude of the EOF mode (no unit).

The time series of the sea level difference between Kushimoto and Uragami is shown in Figure 8, which is an index of the Kuroshio flow path (Moriyasu, 1958, 1961; Kawabe, 1985). We can see a correlation (+0.56) between the sea level difference and the time coefficient of the second mode. This indicates that sea levels at the Southeast Coast station in Figures 6b and 6d become high when the Kuroshio flows in the large-meandering path. We can conclude that the second mode is associated with the Kuroshio Large Meander (LM).

3.4. DENOISING OF TG OBSERVATION

The number of EOFs used is crucial to the denoising: using too few EOFs could result in a lack of information regarding the original sea level variability, whereas using too many could induce additional noise. The RSL were obtained for the period 1993-2020 using EOF decomposition. Then EOF was used for dimensionality reduction by expressing the sea level variability in the linear combination of all the reconstructed TG time series. The first PC explains 82.95 % of the total variance and usually represents the dominant pattern of SLC. The second explains 5.16 %, respectively, of the variance. The EOF decomposition has a fast convergence rate and the total contribution of the PCs is as much as 88.11 %; thus, using these PCs for TG reconstruction should express the characteristics of TG fully. The higher order eigenvectors contain smaller spatial scales and are increasingly affected by noise. In this section, we remain the first and second modes components as primary to minimize the impact of noise, and we designate this method as remain EOF (1+2). The denoised sequence is then re-estimated for velocity, and the results are compared with those obtained using the EMD decomposition denoising method. To ensure consistency with the original velocity, the same software, Hector, is used for velocity estimation (Bos et al., 2013). The results are as follows:

Figures 9 (a, b, c) shows the time series before and after denoising for the TG station 134. Panel (d) displays the periodicity in the TG series obtained from the EMD method at TG station 134 and the EOF reconstruction method (retaining the first two main modes). In the signal power of the EOF reconstruction

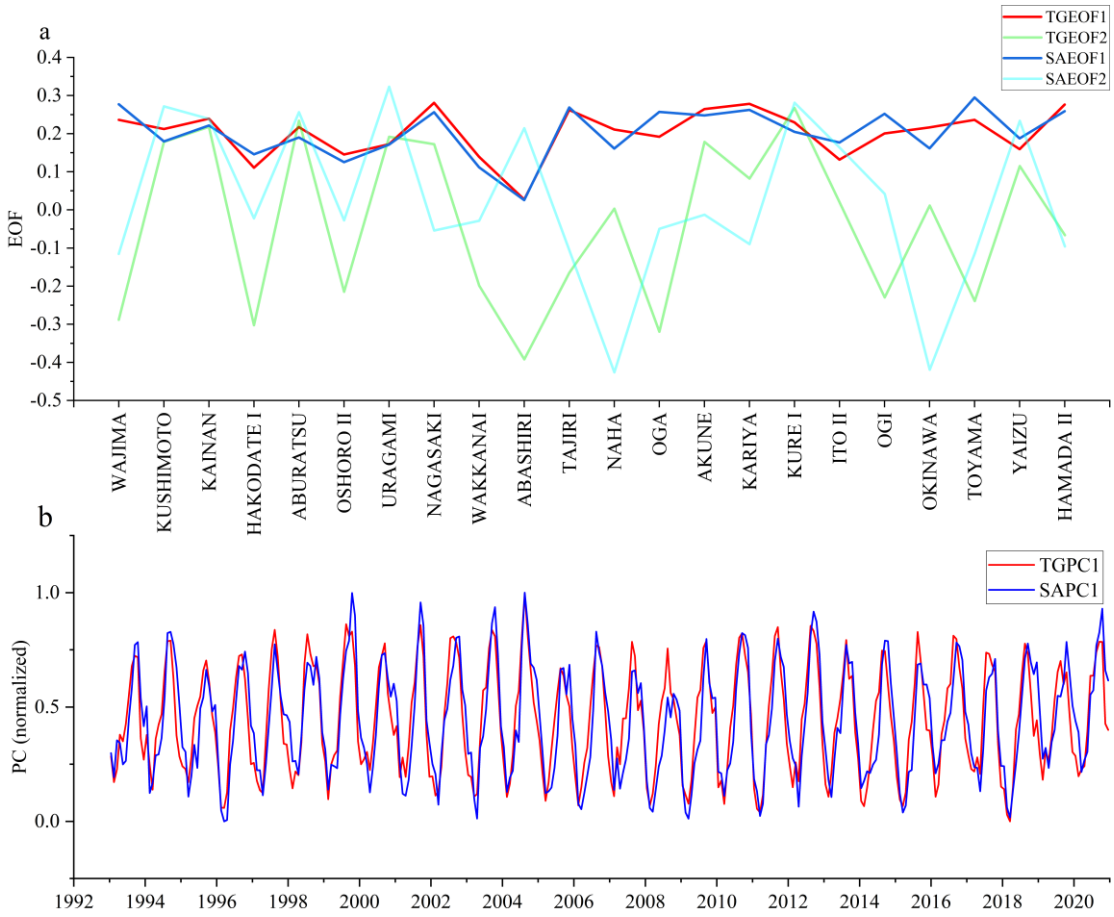

Fig. 7 Eigenvectors of the first and second mode for the TG, SA at the 22 stations. b, PC1 analysis shows only relative intensity (non-dimension values normalized by standard deviations).

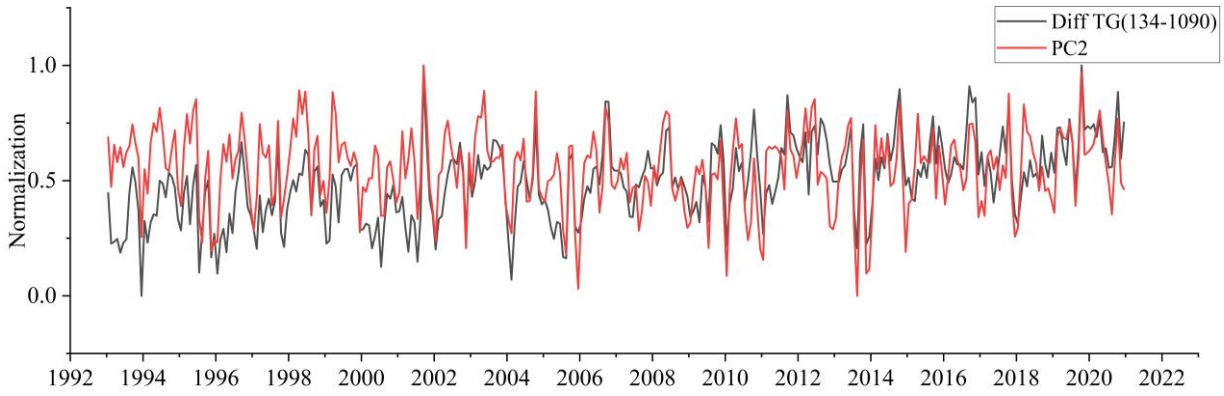

Fig. 8 Principal component of the second modes for the modeled TGs at the 22 tide gauge stations (red). Black time series of the sea level difference of Kushimoto (ID134) minus Uragami (ID1090) in the period from January 1993 to December 2020.

results was suppressed for frequencies less than six month, meaning that the EOF method tends to be less prone to high-frequency sea level variations after denoising the TG measurements. This effectively reduces the noise in the signals of TG records. Moreover, at lower periods, the effectiveness of the EMD method deviates significantly from the original signal. This may be due to the limitations of EMD decomposition, which is restricted to data driven approach denoising and cannot remove noise based on the underlying mechanisms influencing the data. As a result, it may inadvertently discard valuable information contained within the data. This is also evident in Figure 9b, where the time series after EMD noise reduction appears relatively smooth, indicating that a considerable amount of information has been lost from the data.

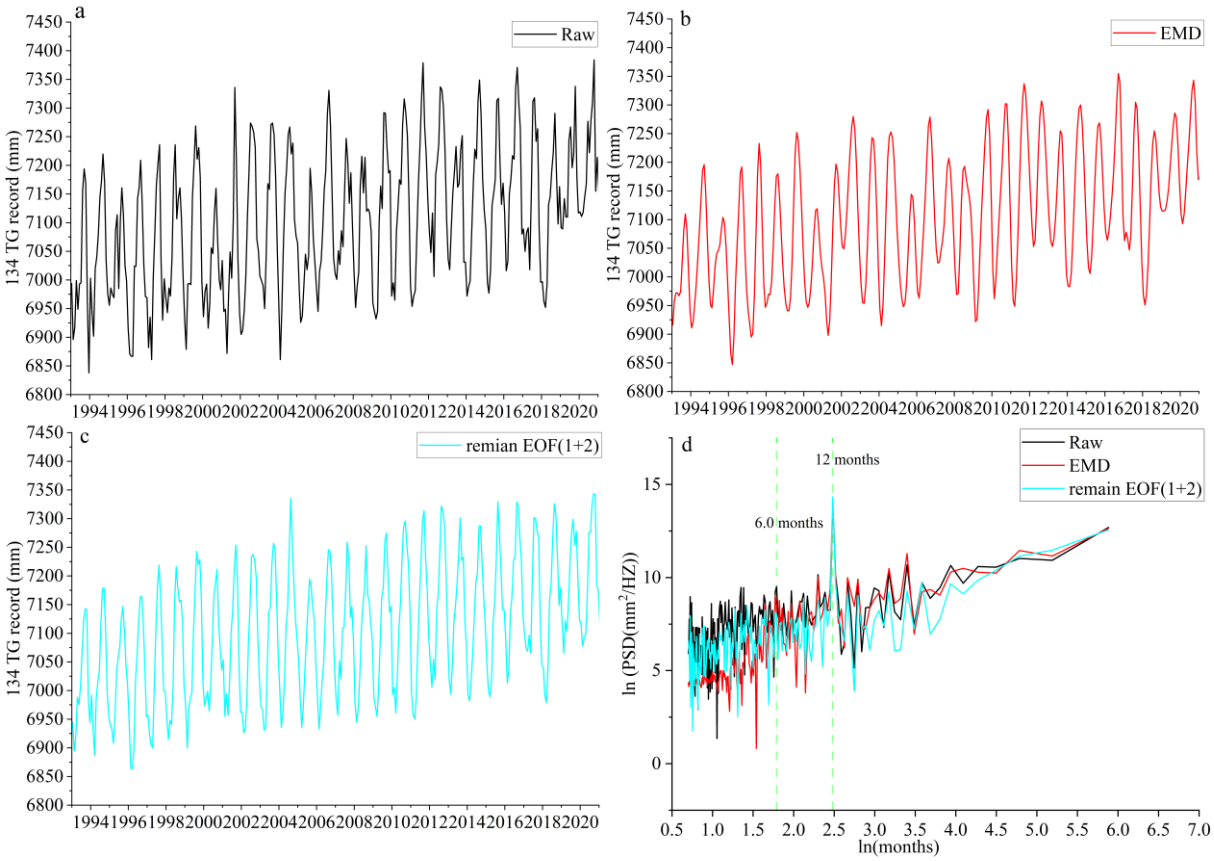

Fig. 9 (a) Raw time series (b) EMD noise reduction time series (c) TG remain EOF (1+2) noise reduction (d) power spectral density (PSD) of using EMD and remain EOF (1+2) at TG station 134. The green dashed lines correspond to the annual and semi-annual periodicity.

In contrast to the geodetic measurements of crustal movement that have been the focus of much of the research into the effects of time-correlated noise in time series, there are well-known quasi-periodic cycles that affect sea level time series at interannual and decadal periods including El Nino-Southern Oscillation and the Pacific Decadal Oscillation (e.g. Hamlington et al., 2013; Wang et al. 2025). Longer-term sea-level variations from these oceanic processes clearly impact the estimation of the underlying rate of sea level change beyond the impacts of variation in annual periodic signals (Zhang and Church, 2012). In fact, it is difficult to assess whether the natural variability has been completely separated from the forced, or anthropogenic, response. This is particularly problematic in the possible case that the forced pattern resembles patterns associated with natural variability (Hamlington et al., 2016; Hamlington et al., 2019). This study explores the significance of the first two modes based on EOF decomposition, performing denoising while preserving the useful components of the data. The results (see Fig. 10 and Table 4) demonstrate that for the 22 stations, the RMS decreased by an average of 6.98 mm compared with the original data when retaining the first two principal components, with the RSL uncertainty reduced by an average of 0.25 mm/a. This approach outperforms the results obtained from EMD decomposition, as detailed in Appendix Table A. These findings suggest that the proposed method effectively removes noise from TG data, thereby improving the accuracy of RSL trend estimates. Unlike the EMD method, EOF decomposition provides a physically interpretable basis for sea level variability, making it a more scientifically robust approach for denoising TG data.

CONCLUSION

In this paper, we utilized SA data and 22 TG stations along the coast of Japan from 1993 to 2020 to analyze sea level changes around the Sea of Japan. The corresponding RSL recorded at TG stations was corrected using GNSS measurements. To further investigate the spatiotemporal variability of sea level in this region, we applied EOF decomposition to both SA and TG data to extract the spatial and temporal modes. By testing the physical significance of each mode, high-frequency noise modes were removed to reduce the uncertainty in sea level trend estimation. The following conclusions can be drawn from the study.

1. The estimated average RSLC rate along the Japanese coast is 2.20 ± 0.62 mm/a, while the ASLC rate derived from satellite altimetry is 3.13 ± 1.66 mm/a, yielding a difference of

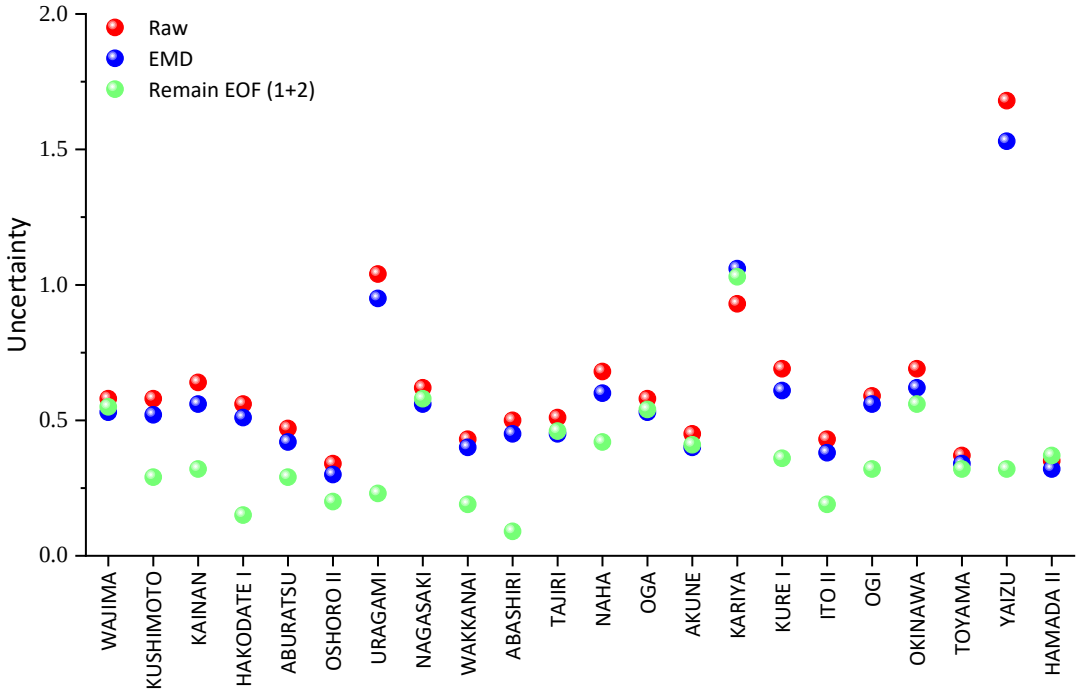

Fig. 10 Comparison of rate uncertainty at 22 TG stations before and after denoising.

Table 4 Denoising performance of the two methods on the raw TG time series.

Index \ Method	EMD	Remain EOF (1+2)
RMS reduction (%)	100	100
Average RMS reduction (mm)	6.95	6.98
Average uncertainty reduction (mm/a)	0.05	0.25

0.93 mm/a. The ASLC rate is notably higher along the southeastern coast compared to other regions. In this study, the SLC rates observed at eight TG stations were significantly lower than those at other stations, with six stations recording negative values. It was verified that the strong VLM uplift in these areas was the primary cause of the declining trend in RSL. After correcting the RSLC, the results showed an average difference of 0.64 mm/a compared to the ASLC calculated from SA.

2. To further elucidate the spatial and temporal variability of sea level in the Sea of Japan, EOF was employed to perform dimensionality reduction on both TG and SA datasets. The TG and SA data exhibited similar spatial and temporal patterns, indicating a high degree of consistency and similarity in the primary sea level changes derived from both datasets. The variance contribution rates of the first two modes were 80.24-82.95 % and 5.16-6.43 %, respectively. The first mode of the EOF for coastal sea level variation represents a simultaneous SLC along the entire Japanese coastline. The second mode is closely related to the LM and this pronounced spatial dependency of the coastal SLC around Japan is not influenced by VLM.
3. We combined the previously discussed modal analysis to interpret the meaning of the modes, selecting the primary modes that reflect SLC. The results indicated that the method is less sensitive to high-frequency sea level variations after Denoising the TG measurements. This effectively reduces the noise in the signals of TG records. The RMS of the denoised sea level time series decreased by an average of 6.98 mm, while the uncertainty in the RSLC rate was reduced by an average of 0.25 mm/a.

ACKNOWLEDGMENTS

This research was supported by the Graduate Innovation Special Fund Project of Jiangxi Province (Grant Nos. YC2024-S552 and YC2024-S553). The authors would like to express their sincere gratitude to Prof. Xiaoxing He and Dr. Shengdao Wang for their valuable assistance in data processing, analysis, and enlightening discussions, which greatly contributed to the improvement of this work.

DECLARATION OF COMPETING INTEREST

The authors declare that they have no known competing financial interests or personal relationships that could have appeared to influence the work reported in this paper.

APPENDIX TABLE A

RSL Trends and RMS from Raw Data, Remain EOF (1+2), and EMD noise reduction

TG	TG	RSL TG	RSL Remain EOF (1+2)	RSL EMD	RMS(Raw) mm	RMS(EMD) mm	RMS Remain EOF (1+2) mm
WAJIMA	132	2.34±0.58	2.50±0.55	2.66±0.53	136.57	126.82	129.11
KUSHIMOTO	134	5.99±0.58	6.38±0.29	6.37±0.52	166.03	161.40	161.28
KAINAN	701	-0.44±0.64	-0.09±0.32	-0.10±0.56	132.36	125.22	125.89
HAKODATE I	813	-4.21±0.56	-4.28±0.15	-4.31±0.51	116.33	113.10	108.27
ABURATSU	814	3.44±0.47	3.67±0.29	3.67±0.42	118.17	110.04	111.28
OSHORO II	1027	0.58±0.34	0.66±0.20	0.67±0.30	115.01	110.24	109.97
URAGAMI	1090	7.37±1.04	8.09±0.23	8.30±0.95	167.33	164.45	158.67
NAGASAKI	1100	4.18±0.62	4.32±0.58	4.35±0.56	152.73	141.34	149.06
WAKKANAI	1103	2.70±0.43	2.84±0.19	2.86±0.40	136.48	131.97	132.19
ABASHIRI	1104	0.69±0.50	0.44±0.09	0.40±0.45	97.58	70.81	75.01
TAJIRI	1148	5.34±0.51	5.70±0.46	5.72±0.45	175.55	166.51	172.93
NAHA	1151	3.07±0.68	2.78±0.42	2.75±0.60	141.00	134.64	126.67
OGA	1264	-1.26±0.58	-0.88±0.54	-0.92±0.53	170.82	167.28	165.18
AKUNE	1265	3.16±0.45	3.32±0.41	3.33±0.40	152.08	144.01	148.60
KARIYA	1318	3.05±0.93	3.55±1.03	3.61±1.06	141.27	134.66	137.78
KURE I	1320	-0.91±0.69	-0.60±0.36	-0.62±0.61	200.33	193.69	194.74
ITO II	1343	-2.76±0.43	-2.07±0.19	-1.98±0.38	573.54	572.29	571.64
OGI	1344	-1.84±0.59	-1.79±0.32	-2.04±0.56	110.15	103.35	100.40
OKINAWA	1388	3.06±0.69	2.59±0.56	2.65±0.62	123.34	118.17	108.64
TOYAMA	1389	3.70±0.37	3.90±0.32	3.91±0.34	151.02	146.77	147.61
YAIZU	1438	5.94±1.68	6.22±0.32	6.70±1.53	166.31	162.43	157.40
HAMADA II	1585	5.16±0.35	5.46±0.37	5.46±0.32	161.71	153.70	159.77

REFERENCES

Adebisi, N., Balogun, A.L., Min, T.H. and Tella, A.: 2021, Advances in estimating sea level rise: A review of tide gauge, satellite altimetry and spatial data science approaches. Ocean Coast. Manag., 208, 105632. DOI: 10.1016/j.ocecoaman.2021.105632

Ballu, V., Gravelle, M., Wöppelmann, G., de Viron, O., Rebischung, P., Becker, M. and Sakic, P.: 2019, Vertical land motion in the Southwest and Central Pacific from available GNSS solutions and implications for relative sea levels. Geophys. J. Int., 218, 3, 1537–1551. DOI: 10.1093/gji/ggz247

Bessières, L., Rio, M.H., Dufau, C., Boone, C. and Pujol, M.I.: 2013, Ocean state indicators from MyOcean altimeter products. Ocean Sci., 9, 3, 545–560. DOI: 10.5194/os-9-545-2013

Bitharis, S., Ampatzidis, D., Pikridas, C., Fotiou, A., Rossikopoulos, D. and Schuh, H.: 2017, The role of GNSS vertical velocities to correct estimates of sea level rise from tide gauge measurements in Greece. Mar. Geod., 40, 5, 297–314. DOI: 10.1080/01490419.2017.1322646

Blewitt, G., Hammond, W. and Kreemer, C.: 2018, Harnessing the GPS data explosion for interdisciplinary science. Eos, 99, 2, e2020943118. DOI: 10.1029/2018eo104623

Boretti, A.: 2024, Sea level patterns around Korea and Japan. Reg. Stud. Mar. Sci., 78, 103720. DOI: 10.1016/j.rsma.2024.103720

Bos, M.S., Fernandes, R.M.S., Williams, S.D.P. and Bastos, L.: 2013, Fast error analysis of continuous GNSS observations with missing data. J. Geod., 87, 4, 351–360. DOI: 10.1007/s00190-012-0605-0

Bos, M.S., Williams, S.D.P., Araújo, I.B. and Bastos, L.: 2014, The effect of temporal correlated noise on the sea level rate and acceleration uncertainty. Geophys. J. Int., 196, 3, 1423–1430. DOI: 10.1093/gji/ggt481

Boudraa, A.O., Cexus, J.C. and Saidi, Z.: 2004, EMD-based signal noise reduction. Int. J. Signal Process., 1, 1, 33–37.

Bruni, S., Fenoglio, L., Raicich, F. and Zerbini, S.: 2022, On the consistency of coastal sea-level measurements in the Mediterranean Sea from tide gauges and satellite radar altimetry. J. Geod., 96, 6, 41. DOI: 10.1007/s00190-022-01626-9

Burgette, R.J., Watson, C.S., Church, J.A., White, N.J., Tregoning, P. and Coleman, R.: 2013, Characterizing and minimizing the effects of noise in tide gauge time series: relative and geocentric sea level rise around Australia. Geophys. J. Int., 194, 2, 719–736. DOI: 10.1093/gji/ggt131

Carson, M., Köhl, A., Stammer, D., Meyssignac, B., Church, J., Schröter, J., ... and Hamlington, B.: 2017, Regional sea level variability and trends, 1960–2007: A comparison of sea level reconstructions and ocean syntheses. J. Geophys. Res., Oceans, 122, 11, 9068–9091. DOI: 10.1002/2017JC012992

Cazenave, A., Gouzenes, Y., Birol, F., Leger, F., Passaro, M., Calafat, F. M., ... and Benveniste, J.: 2022, Sea level along the world's coastlines can be measured by a network of virtual altimetry stations. Commun. Earth Environ., 3, 1, 117. DOI: 10.1038/s43247-022-00448-z

Chepurin, G.A., Carton, J.A. and Leuliette, E.: 2014, Sea level in ocean reanalyses and tide gauges. J. Geophys. Res., Oceans, 119, 1, 147–155. DOI: 10.1002/2013JC009365

Church, J.A. and White, N.J.: 2006, A 20th century acceleration in global sea‐level rise. Geophys. Res. Lett., 33, 1. DOI: 10.1029/2005GL024826

Clark, P.U., Church, J.A., Gregory, J.M. and Payne, A.J.: 2015, Recent progress in understanding and projecting regional and global mean sea level change. Curr. Clim. Change Rep., 1, 224–246. DOI: 10.1007/s40641-015-0024-4

Dangendorf, S., Sun, Q., Wahl, T., Thompson, P., Mitrovica, J. and Hamlington, B.: 2024, Probabilistic reconstruction of sea-level changes and their causes since 1900. Earth Syst. Sci. Data Discuss., 16, 7, 3471-3494. DOI: 10.5194/essd-16-3471-2024

Halliwell Jr, G.R. and Allen, J.S.: 1984, Large-scale sea level response to atmospheric forcing along the west coast of North America, summer 1973. J. Phys. Oceanogr., 14, 5, 864–886. DOI: 10.1175/1520-0485(1984)014

Hamlington, B.D., Bellas-Manley, A., Willis, J.K., Fournier, S., Vinogradova, N., Nerem, R.S., ... and Kopp, R.: 2024, The rate of global sea level rise doubled during the past three decades. Commun. Earth Environ., 51, 601. DOI: 10.1038/s43247-024-01761-5

Hamlington, B.D., Cheon, S.H., Thompson, P.R., Merrifield, M.A., Nerem, R.S., Leben, R.R. and Kim, K.Y.: 2016, An ongoing shift in Pacific Ocean sea level. J. Geophys. Res., Oceans, 121, 7, 5084–5097. DOI: 10.1002/2016JC011815

Hamlington, B.D., Fasullo, J.T., Nerem, R.S., Kim, K.Y. and Landerer, F.W.: 2019, Uncovering the pattern of forced sea level rise in the satellite altimeter record. Geophys. Res. Lett., 46, 9, 4844–4853. DOI: 10.1029/2018GL081386

Hamlington, B.D., Gardner, A.S., Ivins, E., Lenaerts, J.T., Reager, J.T., Trossman, D.S., ... and Willis, M.J.: 2020, Understanding of contemporary regional sea‐level change and the implications for the future. Rev. Geophys., 58, 3, e2019RG000672. DOI: 10.1029/2019RG000672

Hamlington, B.D., Leben, R.R., Strassburg, M.W., Nerem, R.S. and Kim, K.Y.: 2013, Contribution of the Pacific decadal oscillation to global mean sea level trends. Geophys. Res. Lett., 40, 19, 5171–5175. DOI: 10.1002/grl.50950

Hammond, W.C., Blewitt, G., Kreemer, C. and Nerem, R.S.: 2021, GPS imaging of global vertical land motion for studies of sea level rise. J. Geophys. Res., Solid Earth, 126, 7, e2021JB022355. DOI: 10.1029/2021JB022355

Han, M.H. and Lim, H.S.: 2025, Reconstructing sea level variability at the Ieodo Ocean Research Station (1993–2023) using artificial intelligence, machine learning, and reanalysis integration. Earth Syst. Sci. Data Discuss., 1–51. DOI: 10.5194/essd-2025-227

Hannachi, A.: 2004, A primer for EOF analysis of climate data. Department of Meteorology, University of Reading, Reading,1–29.

He, X., Hua, X., Yu, K., Xuan, W., Lu, T., Zhang, W. and Chen, X.: 2015, Accuracy enhancement of GPS time series using principal component analysis and block spatial filtering. Adv. Space Res., 55, 5, 1316–1327. DOI: 10.1016/j.asr.2014.12.016

He, X., Montillet, J.P., Fernandes, R., Bos, M., Yu, K., Hua, X. and Jiang, W.: 2017, Review of current GPS methodologies for producing accurate time series and their error sources. J. Geodyn., 106, 12–29. DOI: 10.1016/j.jog.2017.01.004

He, X., Montillet, J.P., Fernandes, R., Melbourne, T.I., Jiang, W. and Huang, Z.: 2022b, Sea level rise estimation on the Pacific coast from Southern California to Vancouver Island. Remote Sens., 14, 17, 4339. DOI: 10.3390/rs14174339

He, X., Montillet, J.P., Kermarrec, G., Shum, C.K., Fernandes, R., Huang, J., ... and Schuh, H.: 2024, Space and Earth observations to quantify present-day sea-level change. Adv. Geophys., 65, 1, 125–177. DOI: 10.1016/bs.agph.2024.06.001

He, X., Montillet, J.P., Li, Z., Kermarrec, G., Fernandes, R. and Zhou, F.: 2022a, Recent advances in modelling geodetic time series and applications for earth science and environmental monitoring. Remote Sens., 14, 23, 6164. DOI: 10.3390/rs14236164

Holgate, S. J., Matthews, A., Woodworth, P.L., Rickards, L.J., Tamisiea, M.E., Bradshaw, E., ... and Pugh, J.: 2013, New data systems and products at the permanent service for mean sea level. J. Coast. Res., 29, 3, 493–504. DOI: 10.2112/JCOASTRES-D-12-00175.1

Huang, J., He, X., Hu, S. and Ming, F.: 2025, Impact of offsets on GNSS time series stochastic noise properties and velocity estimation. Adv. Space Res., 75, 4, 3397–-3413. DOI: 10.1016/j.asr.2024.12.016

Huang, J., He, X., Montillet, J.P., Bos, M.S. and Hu, S.: 2024, Enhancing sea level rise estimation and uncertainty assessment from satellite altimetry through spatiotemporal noise modeling. Remote Sens., 16, 8, 1334. DOI: 10.3390/rs16081334

Ito, S.I., Uehara, K., Miyao, T., Miyake, H., Yasuda, I., Watanabe, T. and Shimizu, Y.: 2004, Characteristics of SSH anomaly based on TOPEX/POSEIDON altimetry and in situ measured velocity and transport of Oyashio on OICE. J. Oceanogr., 60, 425–437. DOI: 10.1023/B:JOCE.0000038059.54334.6b

Kabir, M. A. and Shahnaz, C.: 2012, Denoising of ECG signals based on noise reduction algorithms in EMD and wavelet domains. Biomed. Signal Process. Control, 7, 5, 481–489. DOI: 10.1016/j.bspc.2011.11.003

Kawabe, M.: 1985, Sea level variations at the Izu Islands and typical stable paths of the Kuroshio. J. Oceanogr. Soc. Jpn., 41, 307-326. DOI: 10.1007/BF02109238

Kim, K.Y., Hamlington, B. and Na, H.: 2015, Theoretical foundation of cyclostationary EOF analysis for geophysical and climatic variables: concepts and examples. Earth-Sci. Rev., 150, 201–218. DOI: 10.1016/j.earscirev.2015.06.003

Kleinherenbrink, M., Riva, R. and Frederikse, T.: 2018, A comparison of methods to estimate vertical land motion trends from GNSS and altimetry at tide gauge stations. Ocean Sci., 14, 2, 187–204. DOI: 10.5194/os-14-187-2018

Lian, T. and Chen, D.: 2012, An evaluation of rotated EOF analysis and its application to tropical Pacific SST variability. J. Clim., 25, 15, 5361–5373. DOI: 10.1175/JCLI-D-11-00663.1

Montillet, J.P. and Bos, M.S., (Eds.): 2019, Geodetic time series analysis in Earth sciences. Springer Geophysics. DOI: 10.1007/978-3-030-21718-1

Moriyasu, S.: 1958, On the fluctuation of the Kuroshio south of Honshu: The influence of the oceanographic conditions upon the monthly mean sea level. J. Oceanogr. Soc. Jpn., 14, 4, 137–144. DOI: 10.5928/kaiyou1942.14.137

Moriyasu, S.: 1961, On the difference in the monthly sea level between Kushimoto and Uragami, Japan. Oceanogr. Soc. Jpn., 17(4), 197–200. DOI: 10.5928/kaiyou1942.17.197

Nakano, H., Urakawa, S., Sakamoto, K., Toyoda, T., Kawakami, Y. and Yamanaka, G.: 2023, Long-term sea-level variability along the coast of Japan during the 20th century revealed by a 1/10° OGCM. J. Oceanogr., 79, 2, 123–143. DOI: 10.1007/s10872-022-00671-4

Okuno, J.I., Nakada, M., Ishii, M. and Miura, H.: 2014, Vertical tectonic crustal movements along the Japanese coastlines inferred from late Quaternary and recent relative sea-level changes. Quat. Sci. Rev., 91, 42–61. DOI: 10.1016/j.quascirev.2014.03.010

Palmer, M.D., Gregory, J.M., Bagge, M., Calvert, D., Hagedoorn, J.., Howard, T., ... and Spada, G.: 2020, Exploring the drivers of global and local sea‐level change over the 21st century and beyond. Earth's Futur., 8, 9, e2019EF001413. DOI: 10.1029/2019EF001413

Peng, F., Deng, X. and Cheng, X.: 2022, Australian coastal sea level trends over 16 yr of reprocessed Jason Altimeter 20–Hz Data Sets. J. Geophys. Res., Oceans, 127, 3, e2021JC018145. DOI: 10.1029/2021JC018145

Pfeffer, J. and Allemand, P.: 2016, The key role of vertical land motions in coastal sea level variations: A global synthesis of multisatellite altimetry, tide gauge data and GPS measurements. Earth Planet. Sci. Lett., 439, 39–47. DOI: 10.1016/j.epsl.2016.01.027

Qiu, B., Chen, S., Wu, L and Kida, S.: 2015, Wind-versus eddy-forced regional sea level trends and variability in the North Pacific Ocean. J. Clim., 28, 4, 1561–1577. DOI: 10.1175/JCLI-D-14-00479.1

Sakamoto, T.T., Hasumi, H., Ishii, M., Emori, S., Suzuki, T., Nishimura, T. and Sumi, A.: 2005, Responses of the Kuroshio and the Kuroshio Extension to global warming in a high–resolution climate model. Geophys. Res. Lett., 32, 14. DOI: 10.1029/2005GL023384

Sasaki, Y.N., Minobe, S. and Miura, Y.: 2014, Decadal sea‐level variability along the coast of Japan in response to ocean circulation changes. J. Geophys. Res., Oceans, 119, 1, 266–275. DOI: 10.1002/2013JC009327

Sasaki, Y.N., Minobe, S. and Schneider, N.: 2013, Decadal response of the Kuroshio Extension jet to Rossby waves: Observation and thin-jet theory. J. Phys. Oceanogr., 43, 2, 442–456. DOI: 10.1175/JPO-D-12-096.1

Sasaki, Y.N., Washizu, R., Yasuda, T. and Minobe, S.: 2017, Sea level variability around Japan during the twentieth century simulated by a regional ocean model. J. Clim., 30, 14, 5585–5595. DOI: 10.1175/JCLI-D-16-0497.1

Senjyu, T., Matsuyama, M. and Matsubara, N.: 1999, Interannual and decadal sea-level variations along the Japanese coast. J. Oceanogr., 55, 619–633. DOI: 10.1023/A:1007844903204

Thompson, P.R., Hamlington, B.D., Landerer, F.W. and Adhikari, S.: 2016, Are long tide gauge records in the wrong place to measure global mean sea level ri*se*? Geophys. Res. Lett., 43, 19, 10–403. DOI: 10.1002/2016GL070552

Uchida, H. and Imawaki, S.: 2008, Estimation of the sea level trend south of Japan by combining satellite altimeter data with in situ hydrographic data. J. Geophys. Res., Oceans, 113, C9. DOI: 10.1029/2008JC004796

Usui, N., Wakamatsu, T., Tanaka, Y., Hirose, N., Toyoda, T., Nishikawa, S. and Kamachi, M.: 2017, Four-dimensional variational ocean reanalysis: a 30-year high-resolution dataset in the western North Pacific (FORA-WNP30). J. Oceanogr., 73, 205–233. DOI: 10.1007/s10872-016-0398-5

Wallace, J.M.: 1972, Empirical orthogonal representation of time series in the frequency domain. Part II: Application to the study of tropical wave disturbances. J. Appl. Meteorol., 11, 6, 893–900.

Wang, S., Shum, C.K., Bevis, M., He, X., Zhang, Y., Ding, Y., ... and Montillet, J.P.: 2025, Sea level reconstruction reveals improved separations of regional climate and trend patterns over the last seven decades. Earth Syst. Sci. Data Discuss., 1–36. DOI: 10.5194/essd-2025-251

Wilks, D.S.: 2011, Principal component (EOF) analysis. Int. Geophys., 100, 519–562. DOI: 10.1016/B978-0-12-385022-5.00012-9

Woodworth, P.L., Melet, A., Marcos, M., Ray, R.D., Wöppelmann, G., Sasaki, Y.N., ... and Merrifield, M.A.: 2019, Forcing factors affecting sea level changes at the coast. Surv. Geophys., 40, 6, 1351–1397. DOI: 10.1007/s10712-019-09531-1

Wöppelmann, G. and Marcos, M.: 2016, Vertical land motion as a key to understanding sea level change and variability. Rev. Geohys., 54, 1, 64–92. DOI: 10.1002/2015RG000502

Wu, X., Zhao, Y., Han, G., Li, W., Shao, Q., Cao, L. and Li, C.: 2022, Temporal-spatial oceanic variation in relation with the three typical Kuroshio paths south of Japan. Acta Ocean. Sin., 41, 2, 15–25. DOI: 10.1007/s13131-021-1941-9

Yasuda, T. and Sakurai, K.: 2006, Interdecadal variability of the sea surface height around Japan. Geophys. Res. Lett., 33, 1. DOI: 10.1029/2005GL024920

Zhang, X. and Church, J.A.: 2012, Sea level trends, interannual and decadal variability in the Pacific Ocean. Geophys. Res. Lett., 39, 21. DOI: 10.1029/2012GL053240

Zhou, D., Liu, Y., Feng, Y., Zhang, H., Fu, Y., Liu, Y. and Tang, Q.: 2022, Absolute sea level changes along the coast of China from tide gauges, GNSS, and satellite altimetry. J. Geophys. Res., Oceans, 127, 9, e2022JC018994. DOI: 10.1029/2022JC018994

Zhou, Y., He, X., Montillet, J.P., Wang, S., Hu, S., Sun, X., ... and Ma, X.: 2025, An improved ICEEMDAN-MPA-GRU model for GNSS height time series prediction with weighted quality evaluation index. GPS Solut., 29, 3, 1–19. DOI: 10.1007/s10291-025-01867-z

Zhu, H., Chen, K., Chai, H., Ye, Y. and Liu, W.: 2024, Characterizing extreme drought and wetness in Guangdong, China using global navigation satellite system and precipitation data. Sat. Nav., 5, 1, 1. DOI: 10.1186/s43020-023-00121-6

Zhu, H., Chen, K., Hu, S., Liu, J., Shi, H., Wei, G., ... and Wang, T.: 2023, Using the global navigation satellite system and precipitation data to establish the propagation characteristics of meteorological and hydrological drought in Yunnan, China. Water Resour. Res., 59, 4, e2022WR033126. DOI: 10.1029/2022WR033126